MNRAS 000, 1–9 (2017) Preprint 8 January 2018 Compiled using MNRAS LATEX style file v3.0

Extinction and time-delay constraints from the first resolved strongly lensed Type Ia supernova iPTF16geu

R. Amanullah,[1]★ A. Goobar,[1] B. Cenko, A. Cooray, O. Fox, R. Kalender,[1]
M. Kasliwal, E. Mörtsell,[1] H. Nayyeri
[1]*The Oskar Klein Centre, Physics Department, Stockholm University, Albanova University Center, SE 106 91 Stockholm, Sweden*

Accepted XXX. Received YYY; in original form ZZZ

ABSTRACT
Observations of resolved strongly lensed Type Ia supernovae (SNe Ia) can be used for cosmological applications or to study properties of the lensing galaxy, such as extinction and the matter distribution . Here we report the results from measurements obtained with the Hubble Space Telescope of the multiple images of iPTF16geu.

Key words: keyword1 – keyword2 – keyword3

1 INTRODUCTION

More than half a century has passed since Refsdal (1964) proposed to measure the expansion rate of the universe, the Hubble parameter, using time delay measurements of multiply-imaged gravitationally lensed supernovae (SNe). However, discovering these rare events has proven very challenging and it is only thanks to the recent developments in time domain astronomy that the first couple of resolved lensed supernovae have been detected. SN Refsdal (Kelly et al. 2015), detected with the Hubble Space Telescope (HST), is a core-collapse SN magnified by a cluster of galaxies, while iPTF16geu (Goobar et al. 2017), the subject of this work, is split into four resolved images by an individual galaxy. Furthermore, it was spectroscopically classified as a Type Ia supernova, i.e., it is well-suited to study the magnification caused by the lensing galaxy, as well as the potential dimming of light by attenuation by dust in either the SN host galaxy or in the lens. The discovery of iPTF16geu highlighted the power of the wide-field surveys to discover lensed SNe Ia without the need of high-spatial observations, thanks to their "standard candle" nature. At $z = 0.409$, the SN was found to be 30 standard deviations too bright compared with the SN Ia population, which prompted us to observed the system from space with HST and with adaptive optics (AO) at VLT and Keck. Here we report on the multi-wavelength follow-up observations carried out while the SN was active in late 2016, as well as laser aided AO Near IR observations with Keck after the SN had faded below the detection limit, about a year after explosion.

The data at hand is used to estimate the dimming by dust in the host galaxy, common to all four SN images, and in the lensing galaxy for the individual images. This provides us with unique extinction measurements in the lensing elliptical galaxy at $z = 0.216$ and we use the corrected lightcurves to measure the time delays between the four SN images. The accurate image positions and the corresponding fluxes are used to model the lens. By comparing with the predicted flux ratios from the lens model with the reddening corrected observations we assess the possibility that the residuals are caused by lensing of substructures within the lensing galaxy.

2 OBSERVATIONS

2.1 Hubble Space Telescope Wide Field Camera 3

We observed iPTF16geu with the Hubble Space Telescope (HST) Wide Field Camera 3 (WFC3) in under program DD 14862 (PI: A. Goobar) using the ultra violet (WFC3/UVIS) and (WFC3/IR) channels. For both channels we only read out part, 512×512 pixels, of the full detectors. However, given the different pixel scales of the two channels, $0.04''$/pixel and $0.12''$/pixel for WFC3/UVIS and WFC3/IR, respectively, they will not cover the same area on the sky. The data were obtained using either a 3- or 4-point standard dithering pattern for both channels. For WFC3/UVIS we used the `UVIS2-C512C-SUB`, that is located next to the amplifier, with a post-flash to maximize the charge transfer efficiency (CTE) during read-out. All imaging data are shown in Table 1.

The automatic `calwf3` reduction pipeline at the Space Telescope Science Institute, where the data were dark subtracted, flat-fielded and corrected for charge-transfer inefficiency was used for all data, although different steps are involved for the two channels. The individual images were the combined and corrected for geometric distortion using the `AstroDrizzle` software.

2.2 Ground data

In addition to the data already presented in G17, iPTF16geu was followed from the ground in until it disappeared behind the sun. We further observed the system in *J*, *H* and *Ks* bands on UT June

★ E-mail: rahman@fysik.su.se

Table 1. Hubble Space Telescope Wide Field Camera 3 data imaging data presented here. The columns are the civil date, the Modified Julian Date (MJD), the HST passband, total exposure time, the number of sub-exposures, and the WFC3 camera. The WFC3/UVIS and WFC3/IR data were obtained with the `UVIS2-C512C-SUB` and `IRSUB512` subarray, respectively.

Civil date	MJD (days)	Filter	Exp. (s)	Sub	Camera
2016-10-20	57681.62	F475W	378.0	3	UVIS2
2016-10-20	57681.62	F625W	291.0	3	UVIS2
2016-10-20	57681.63	F814W	312.0	3	UVIS2
2016-10-20	57681.64	F110W	63.9	3	IR
2016-10-20	57681.64	F160W	621.4	3	IR
2016-10-25	57685.91	F625W	198.0	3	UVIS2
2016-10-25	57685.92	F814W	114.0	3	UVIS2
2016-10-25	57685.93	F475W	183.0	3	UVIS2
2016-10-25	57685.94	F390W	429.0	3	UVIS2
2016-10-25	57685.99	F110W	63.9	3	IR
2016-10-25	57685.99	F160W	415.1	3	IR
2016-10-29	57689.89	F475W	378.0	3	UVIS2
2016-10-29	57689.91	F625W	291.0	3	UVIS2
2016-10-29	57689.91	F814W	312.0	3	UVIS2
2016-10-29	57689.96	F110W	63.9	3	IR
2016-10-29	57689.96	F160W	621.4	3	IR
2016-11-02	57694.21	F625W	804.0	4	UVIS2
2016-11-02	57694.21	F814W	480.0	4	UVIS2
2016-11-02	57694.24	F110W	63.9	3	IR
2016-11-02	57694.24	F160W	415.1	3	IR
2016-11-02	57694.28	F105W	309.4	3	IR
2016-11-06	57698.25	F625W	644.0	4	UVIS2
2016-11-06	57698.25	F814W	420.0	4	UVIS2
2016-11-06	57698.26	F110W	63.9	3	IR
2016-11-06	57698.26	F160W	621.4	3	IR
2016-11-10	57702.16	F625W	804.0	4	UVIS2
2016-11-10	57702.16	F814W	480.0	4	UVIS2
2016-11-10	57702.17	F110W	63.9	3	IR
2016-11-10	57702.17	F160W	415.1	3	IR
2016-11-15	57707.12	F625W	644.0	4	UVIS2
2016-11-15	57707.12	F814W	420.0	4	UVIS2
2016-11-15	57707.14	F110W	63.9	3	IR
2016-11-15	57707.14	F160W	621.4	3	IR
2016-11-17	57709.72	F625W	804.0	4	UVIS2
2016-11-17	57709.74	F814W	480.0	4	UVIS2
2016-11-17	57709.78	F110W	63.9	3	IR
2016-11-17	57709.78	F160W	415.1	3	IR
2016-11-22	57714.32	F625W	644.0	4	UVIS2
2016-11-22	57714.32	F814W	420.0	4	UVIS2
2016-11-22	57714.35	F110W	63.9	3	IR
2016-11-22	57714.35	F160W	621.4	3	IR

16th 2017, after the iPTF16geu had faded away, using laser guided adaptive optics (LGS-AO) with the NIRC2 instrument at the Keck II telescope on Mauna Kea. For the *J* and *H* bands we obtained 9 exposures in a dithering pattern, each with an integration time of 20 s. For the *Ks* band, 18 exposures of 65 s were acquired.

Standard near infrared reduction was applied where the individual images were first dark subtracted and flat fielded. The flat frames where obtained using the same dome on-off technique as described in G17. The sky background for each science frame was obtained from the images preceding and following each exposure, after first masking out the object. Together with data presented in G17 this resulted in a total of 3 epochs for the NIRC2/*J* and 2 epochs for the NIRC2/*H* and NIRC2/*Ks* bands, respectively.

3 PHOTOMETRIC ANALYSIS

3.1 Forward modelling of the NIRC2 images

The LGS-AO NIRC2 images have the highest spatial resolution in our data set. This is also the only data with resolved SN images for which reference images[1] without active SN light are available. Reference images are important, but not essential, for obtaining background-subtracted photometry of SNe.

We can use the NIRC2 data to build a parametric model of the iPTF16geu system, including the SN images, the host galaxy, and the lens. The model we use is described in detail in §A, but in summary, the shape of the lensing galaxy is modeled with a Sérsic profile (Sérsic 1963) while the SN images are modeled by the point-spread function (PSF). The shape of the SN host galaxy is described by the expansion in eq. (A2). The full model is then fitted simultaneously to all data in for one NIRC2 filter at a time. Some parameters, such as the host and lens models and the position of the SN images, are forced to be the same for all available images in a filter, while the fluxes of the SN images are allowed to vary between the different epochs.

We generally use the parametrisation by Moffat (1969) for the PSF. When doing PSF photometry it is customary to first use isolated bright stars in the field to fit the PSF shape, and then fix the model. However, since we are lacking isolated stars (or any objects but the iPTF16geu system) in the narrow field of view NIRC2 images, the PSF parameters is fitted together with the rest of the parmeters of the iPTF16geu model, including the SN fluxes. In other words, the SN images is effectively used to determine the PSF shape. We do not allow the PSF shape parameters to vary between the four SN images.

Fitting the PSF shape together with the model will complicate the fitting procedure. While the iPTF16geu model is not expected to vary with time, the observing conditions will, and these are characterised by the differences in the PSFs we are attempting to fit together with the model. We address this by iteratively fitting first the model, and then the PSF shape, to one of our epochs. Once this fit has converged, we use the resulting parameters as initial conditions for the simultaneous fit. For each iteration in the final fitting procedure, the combined model then first convolved with the PSF before it is compared to the data. For the reference images, that are lacking any point-sources, we adopt a Gaussian PSF. The width of the Gaussian is fitted together with the other parameters, and the degeneracy between the Gaussian width and and the background model is broken since the same background model is fitted to all epochs simultaneously.

Examples of data and the fitted models are shown in Figure 1. The fitted positions of the four SN images for the NIRC2 *J*-band are further presented Table 2, while the lens and host parameters are shown in Tables 3–5.

As seen in Figure 1 the model fits the data well in general. Four SN images are clearly visible in the *J*-band but from panel d) we also see that the fit is not perfect. Discrepancies can mainly be seen for the brightest SN image, which are probably due to an imperfect PSF model, rather than an insufficient background model. In other words, if the systematic PSF uncertainties are known, the method can be used to obtain fluxes for the four SN images.

From the radial profile plots in panels f)–i) there is an apparent degeneracy between the host model and the SN profiles given that their extrema coincide and have similar width. However, recall that

[1] Sometimes referred to as template images.

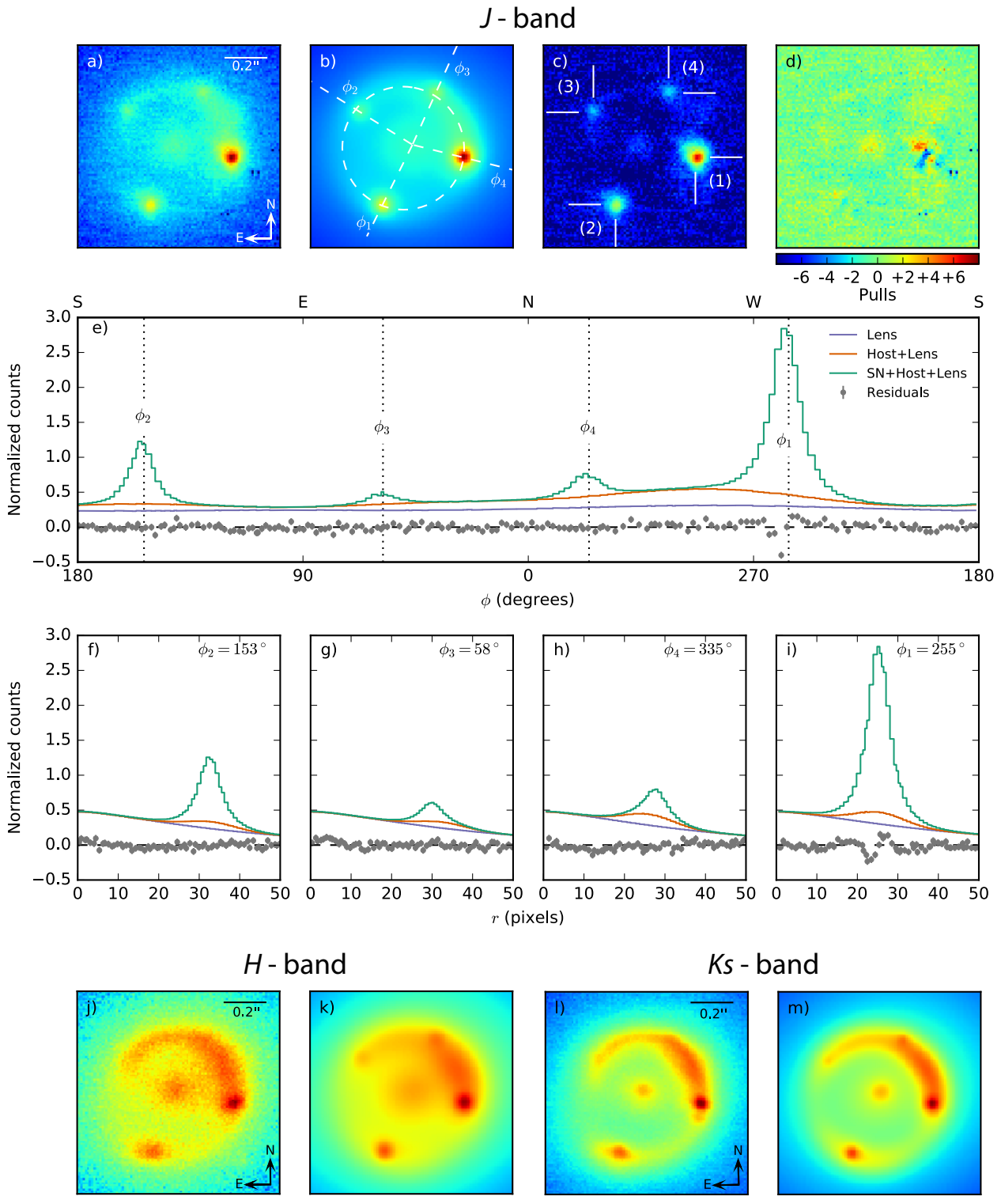

Figure 1. a) NIRC2 *J* image of the iPTF16geu system obtained on on Nov 5, 2016. **b)** The model fitted simultaneously to all available epochs as described in the text. The dashed circle show the position of the host galaxy as described in eq. (A4). The dashed lines are showing the angular positions of the four SN images. **c)** The subtraction between the data and the host and lens models. The fitted PSF positions of the four SN images have been marked. **d)** The "pulls", i.e. the residuals normalized with the pixel uncertainties when the lens, host and SN model is subtracted from the data. **e)** The profile of both the model and the residuals along the host radius marked by the dashed circle in b), The fitted angles, ϕ_i, of the SN images are marked by the dotted, black lines. **f) – i)** The radial profiles from the center for the SN images as marked and labelled in b). **j) – k)** NIRC2 *H* image obtained on Oct 23, 2016 and the corresponding fitted model. **l) – m** NIRC2 *Ks* image obtained on Oct 22, 2016 and the corresponding fitted model.

Table 2. The fitted SN positions to the NIRC2 *J*-band images. The origin is defined as the origin of the iPTF16geu system as it is obtained from the model fit and the angle, $0 \leq \varphi < 2\pi$, is defined from North towards East. All quoted uncertainties are statistical errors obtained from the simultaneous fit described in the text.

Image	r ($''$)	φ (rad)
1	0.251 (0.001)	4.468 (0.002)
2	0.324 (0.001)	2.679 (0.003)
3	0.297 (0.002)	1.013 (0.006)
4	0.276 (0.001)	5.860 (0.005)

we only fit one parameter, σ_H, for the width of the host model, as explained in §A, and the value of this parameter will mainly be determined by the pixels between the images located along the dashed circle in panel b). Further, by studying the profile along this circle, as shown in panel e), we can conclude that the maximum of the host galaxy amplitude appears to be located between images (1) and (4), and the best fit model suggest that the background flux under the SN images is either increasing or decreasing monotonically.

Since we do not expect the image positions to change with neither time nor wavelength, we will fix the positions to the values in Table 2 for the remaining of the analysis in this paper. Using the *J* as the reference, is motivated both by the fact that the ratio between the SN flux and the background is higher than for the other NIRC2 filters, and that we have two epochs where the SN is active.

With the SN positions fixed we move on to fit the host model for the remaining NIRC2 filters. The fitted models to the *H*- and *Ks*-band are shown in panels j)–m) in Figure 1. In the figure, the epochs when the SN was active are shown together with the corresponding data. The lens and host model parameters are presented in Tables 3–5.

3.2 WFC3 photometry

The WFC3 data were obtained while iPTF16geu was active and reference images without SN light are currently not available. However, the photometry of the SN can still be extracted by using a similar approach as in §3.1.

For the data obtained in particular with WFC3/UVIS we face a similar challenge as for NIRC2, the field of view is too small to include any isolated stars that could be used to model the PSF. While conditions in space are relatively stable the PSF of WFC3 do vary both over the focal plane and in time, and a lot of effort has gone into understanding its characteristics (Anderson 2016; Anderson & Bedin 2017). However, here we use a simple approach that is described in detail in § B and only briefly summarised here. For WFC3/UVIS we simultaneously fit the parameters of a Moffat profile to bright stars observed over time with the same subarray as iPTF16geu. The resulting fluxes are then compared to the corresponding values obtained from calibrated aperture photometry, following the prescription outlined in WFC3 data handbook. The calculated estimated standard deviation, 0.02–0.10 mag, from this comparison is used as the uncertainty of the method, and is added to the error budget of the iPTF16geu photometry.

The field-of-view for the WFC3/IR data is larger, and the bright star 20$''$ North of iPTF16geu, was included in all observations. We simultaneously fit a PSF model to all observations of this star, which result in a dispersion < 0.01 mag with respect to the calibrated aperture photometry, if the last epoch is excluded. Since this epoch does not provide a significant contribution to the lightcurve it will also be excluded from the rest of the analysis.

Using one fixed PSF for each filter, we can then follow the procedure from §3.1 and §A. Since we assume that the PSF is the same for all epochs, we do not convolve the model before comparing with the data in the fitting routine, although doing this will result in similar SN fluxes. We also omit the host galaxy component from the model for the two bluest bands, $F390W$ and $F475W$, since data was not deep enough to detect it at these wavelengths. For these filters we also constrained ourselves to a circular symmetric lens model.

While fitting the combined iPTF16geu model works well for WFC3/UVIS it is significantly more challenging for the WFC3/IR data. Both due to the lower resolution and to the flux ratio between the SN images and the background being much lower. The effective radius and the Sérsic index for the lens can be constrained by the light beyond the Einstein right, but there is a degeneracy between the different components inside the ring. We therefore decided to only fit a single normalisation parameter for the host model, and fix all other parameters to the values obtained for the NIRC2 *J* and *H*-fits, given that effective wavelengths of these bands are similar to $F110W$ and $F160W$, respectively. These may be improved once reference images become available.

Examples of data, model and normalised residual patches are shown in Figure 2 for the different WFC3 bands, while the fitted parameters for the background models are presented in Tables 3–5. The fitted host normalisation parameters are shown in Table 6. The resulting SN fluxes from the simultaneous fitting is presented in Table C1.

In Table C1 we present two different errors for each measurement. The first error is the statistical fitting error that is obtained from the simultaneous fit for each filter. However, we cannot exclude there are remaining degeneracies between primarily the host model and the SN fluxes. From the residual patches for $F110W$ and $F160W$ in Figure 2 we can also see that the model we fit here does not provide very good fit to the data. In order to estimate the uncertainties from the background model, we rebin the NIRC2 *J*-band data to pixel scales similar the WFC3/UVIS and WFC3/IR data. We then carry out model fits to the data, both using and omitting the reference image, and can conclude that the background flux within a FWHM radius under the SN images varies within up to 10 % between the two different cases. For each fitted background model to the WFC3 data, we then similarly calculate the underlying background model flux for each SN image, and add 10 % of this value to the error budget. This is shown in the second error column of Table C1.

4 RESULTS

4.1 Time-delays

4.2 Differential extinction

5 CONCLUSIONS

ACKNOWLEDGEMENTS

REFERENCES

Anderson J., 2016, Technical report, Empirical Models for the WFC3/IR PSF
Anderson J., Bedin L. R., 2017, preprint, (arXiv:1706.00386)
Deustua S. e. a., 2016, Technical report
Goobar A., et al., 2017, Science, 356, 291
Kelly P. L., et al., 2015, Science, 347, 1123

Table 3. The fitted lens model parameters as described in eq. (A1). The origin $(x_0^{(n)}, y_0^{(n)})$ of the coordinate system are fitted as free parameters for each image n. Angles are defined as $0 \leq \theta < 2\pi$ from North towards East. All quoted uncertainties are statistical fitting errors from each simultaneous fit. *Note:* Parameters marked with an asterisk (*) were fixed to the given value in the fit.

Filter	f_S	r_e ($''$)	n_S	ε	θ (rad)
J	1.44E−01 (1E−03)	0.528 (0.002)	0.79 (0.01)	0.127 (0.002)	0.19 (0.01)
H	2.08E−01 (2E−03)	0.585 (0.002)	0.84 (0.01)	0.160 (0.002)	0.30 (0.01)
K_s	2.43E−01 (1E−03)	0.544 (0.001)	0.79 (0.00)	0.165 (0.002)	0.35 (0.01)
$F390W$	9.53E−03 (1E−02)	0.337 (0.313)	1.08 (1.05)	*0.000	*0.00
$F475W$	4.76E−02 (2E−02)	0.366 (0.111)	1.10 (0.32)	*0.000	*0.00
$F625W$	1.12E−01 (5E−03)	0.570 (0.020)	1.37 (0.04)	0.236 (0.006)	0.18 (0.01)
$F814W$	2.12E−01 (7E−03)	0.501 (0.012)	1.12 (0.03)	0.221 (0.005)	0.20 (0.01)
$F110W$	1.99E+01 (7E−01)	0.460 (0.009)	1.43 (0.04)	*0.127	*0.19
$F160W$	1.28E+01 (4E−01)	0.476 (0.007)	1.38 (0.03)	*0.160	*0.30

Table 4. The fitted parameters of the host model, defined in (A2). All quoted uncertainties are statistical fitting errors from each simultaneous fit.

Filter	a_0	a_1	b_1	a_2	b_2
J	2.78E−01 (5E−03)	−6.93E−02 (2E−03)	4.75E−02 (2E−03)	−3.43E−02 (1E−03)	−1.52E−02 (1E−03)
H	5.16E−01 (3E−03)	−1.07E−01 (2E−03)	8.64E−02 (2E−03)	−4.76E−02 (1E−03)	1.75E−03 (2E−03)
K_s	1.47E+00 (1E−02)	−2.97E−01 (3E−03)	2.56E−01 (3E−03)	−1.41E−01 (2E−03)	3.53E−02 (2E−03)
$F625W$	3.29E−01 (6E−03)	2.65E−02 (4E−03)	1.04E−02 (3E−03)	−3.97E−02 (4E−03)	−1.00E−02 (4E−03)
$F814W$	6.81E−01 (9E−03)	−5.74E−02 (5E−03)	5.56E−02 (5E−03)	−8.65E−02 (5E−03)	−3.44E−02 (5E−03)

Filter	a_3	b_3	c_0 ($''$)	c_1 ($''$)	d_1 ($''$)
J	3.46E−02 (1E−03)	−2.00E−02 (1E−03)	5.911E−01 (1E−03)	4.49E−02 (1E−03)	−1.69E−02 (9E−04)
H	5.72E−02 (2E−03)	−4.73E−02 (2E−03)	5.787E−01 (8E−04)	3.38E−02 (8E−04)	−3.11E−02 (8E−04)
K_s	1.76E−01 (2E−03)	−1.63E−01 (3E−03)	5.831E−01 (3E−04)	3.08E−02 (3E−04)	−3.54E−02 (3E−04)
$F625W$	3.44E−03 (4E−03)	−4.47E−02 (3E−03)	5.598E−01 (2E−03)	3.24E−02 (2E−03)	6.38E−03 (1E−03)
$F814W$	4.30E−02 (5E−03)	−7.77E−02 (4E−03)	5.682E−01 (1E−03)	3.98E−02 (1E−03)	−6.40E−03 (1E−03)

Table 5. The fitted widths, σ_H, for the host model defined in eq. (A2).

Filter	σ_H ($''$)
J	0.102 (0.003)
H	0.129 (0.001)
K_s	0.080 (0.001)
$F625W$	0.123 (0.003)
$F814W$	0.119 (0.002)

Table 6. The fitted normalisation parameter, h, for the host model in eq. (A2) for the WFC3/IR bands. In this case the parameters a_i, b_i are kept fixed to the values obtained for the NIRC2 J and H bands, respectively.

Moffat A. F. J., 1969, A&A, 3, 455
Refsdal S., 1964, MNRAS, 128, 307
Sérsic J. L., 1963, Boletin de la Asociacion Argentina de Astronomia La Plata Argentina, 6, 41

APPENDIX A: FORWARD MODELLING OF THE iPTF16geu IMAGES

A model, $F(r, \phi)$, of the observed 2D shape of the iPTF16geu system in a broadband image, can be expressed as a combination of parametric lens and host models, $L(r, \phi)$ and $H(r, \phi)$, and the point spread function (PSF) of the image as

$$F(r,\phi) = A_n \cdot PSF \otimes [L(r,\phi) + H(r,\phi)] + \\ + \sum_{i=1}^{4} \left(f_i^{(n)} PSF(r_i, \phi_i) \right) + B_n$$

where the coordinates (r, ϕ) are defined with respect to the center (which are treated as nuisance parameters in the fit) of the system in each image n, and the angle $0 \leq \phi < 2\pi$ runs from North towards East. The index, $i = 1, 2, 3, 4$ runs over the four SN images, and n runs over all observed epochs for a given band. Further, $f_i^{(n)}$ and (r_i, ϕ_i) are the fluxes and coordinates of the SN images. The amplitude, A_n, can be used to account for varying photometric calibration, but must be kept fixed for at least one image in each band in order to break the degeneracy between the parameters for L and H. We also allow for the background, B_n to vary between images.

The lens, L, is modelled by a Sérsic profile (Sérsic 1963)

$$L(r,\phi) = S^{n_S}(r,\phi) = f_S \cdot \exp\left\{ -b_n \left[\left(\frac{r_S(\theta, \epsilon; \phi)}{r_e} \right)^{\frac{1}{2n_S}} - 1 \right] \right\} \quad \text{(A1)}$$

Figure 2. Examples of data, model and residual patches for each WFC3 filter. The residual patches have been normalised by the pixel uncertainty to form the "pull". For each filter, the epoch where the SN was the brightest is shown. This corresponds to Oct. 20, 2016 for $F475W$, $F625W$, and $F814W$, Oct. 25, 2016 for $F390W$, and Nov. 2nd, 2016 for $F110W$ and $F160W$, respectively.

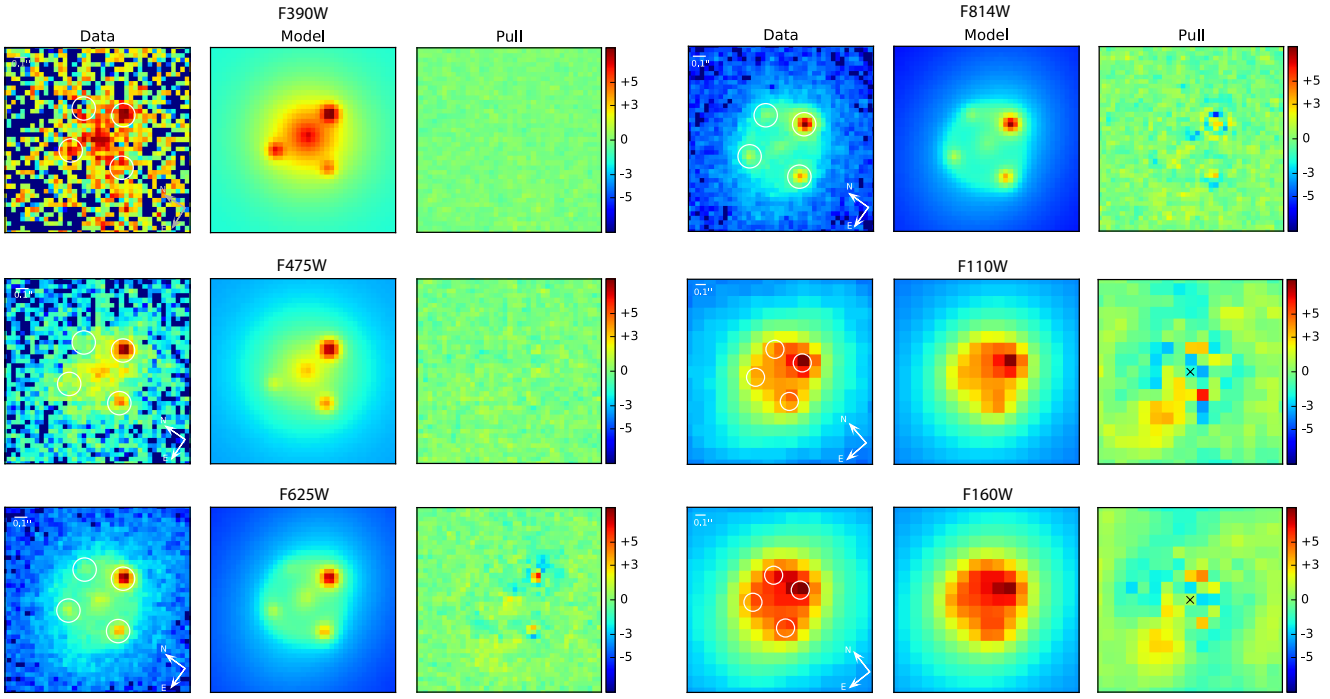

where $r_S(\theta, \epsilon; \phi)$, is generalized to allow for an elliptical model with ellipticity, ϵ, and rotation, θ. Here, b_n (solved for numerically) is defined such that r_e contains half of the total luminosity , f_S is the intensity, and n_S is the Sérsic index.

The host galaxy is expressed as a Gaussian profile according to

$$H(x, y) = h \cdot f_H(\phi) \cdot \exp\left\{-\frac{(r - r_H(\phi))^2}{2\sigma_H^2}\right\}, \quad \text{(A2)}$$

where the amplitude, $f_H(\phi)$ and radius, $r_H(\phi)$ are defined as

$$f_H(\phi) = \frac{a_0}{2} + \sum_{j=1}^{3} a_j \cdot \sin(j\phi) + b_j \cdot \cos(j\phi), \quad \text{(A3)}$$

$$r_H(\phi) = \frac{c_0}{2} + c_1 \cdot \sin(\phi) + d_1 \cdot \cos(\phi). \quad \text{(A4)}$$

The parameter h, and the parameters a_0, a_j, b_j cannot be fitted simultaneously. The former is only allowed as a free parameter for WFC3/IR when a_0, a_j, b_j is fixed to the solution for the LGS-AO data.

We also allow for a rotation, δ_n of the full system, i.e. $\phi \rightarrow \phi + \delta_n$ between images. These parameters must be fixed for at least one image to break the degeneracy with the angle dependent model parameters.

In its most general implementation the number of free parameters of the model can be:

- $2 \times n + (n - 1)$ for the position and rotation in each image
- $4 \times 3 \times n$ for the SN fluxes and positions
- $n - 1$ for the normalization of the model in each image
- 5 for the lens model
- 11 for the host model

which results in a total of $14 + 16n$ parameters. However, when fitting this model to the data we will generally require that the SN positions are the same between different filters.

APPENDIX B: EMPIRICAL POINT-SPREAD FUNCTION MODEL FOR WFC3

Although the shape and variability of the point-spread-function (PSF) of WFC3 has been studied in great detail (Anderson 2016; Anderson & Bedin 2017), a simple time-independent PSF model will be used here. We fit the profile,

$$PSF(x, y; A, \alpha, \gamma) = A \cdot \frac{\alpha - 1}{\pi\gamma^2}\left[1 + \left(\frac{x^2 + y^2}{\gamma^2}\right)\right]^{-\alpha},$$

as described by Moffat (1969), where, x and y are pixel coordinates and A, α and γ are free parameters. The profile is fitted to bright isolated stars observed between 2010 and 2017 and with the same subarray, `UVIS2-C512C-SUB`, used for the iPTF16geu. The data are also drizzled to the same resolution, and with the same kernel as for our science observations.

The WFC3/IR observations of iPTF16geu was obtained with a larger field-of-view than WFC3/UVIS as shown in Fig. B1, and included a bright, but unsaturated, star $\sim 20''$ North of the object. The star was visible in all WFC3/IR and bands and could be used to determine the PSF shape for these filters using the same approach as for WFC3/UVIS.

The PSF fit is carried out to all data in a given filter. While the amplitude, A, is fitted to each exposure, the parameters, α and γ, are only allowed to vary between different filters. The fitted amplitudes of each star are then compared to the corresponding value obtained from aperture photometry. For the latter we follow the guidelines in the WFC3 data handbook (Deustua 2016) and always use a fixed aperture radius of $0.4''$, for which zero points

Table B1. Table of the derived PSF parameters and the estimated standard deviations PSF and aperture photometry for all stars in each given. Here, the full width at half maximum was calculated as FWHM = $2\gamma\left(2^{1/\alpha}-1\right)^{1/2}$. See the text for further details.

Band	α	γ (pix)	FWHM (pix)	σ (mag)
F390W	3.245	2.398	2.340	0.072
F475W	3.114	2.531	2.528	0.096
F625W	1.844	1.592	2.151	0.083
F814W	1.798	1.414	1.939	0.024
F110W	2.929	1.343	1.388	0.007
F160W	2.646	1.327	1.452	0.006

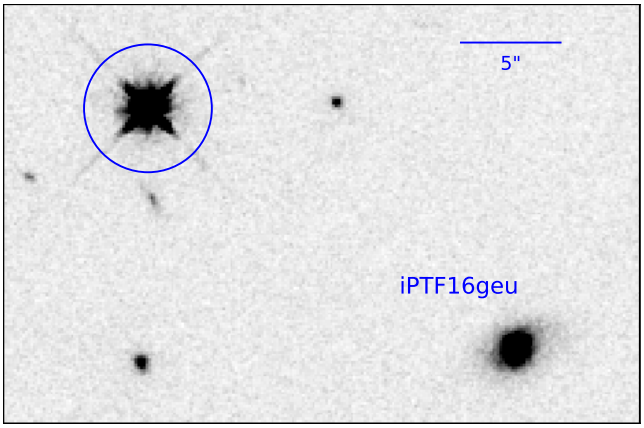

Figure B1. Observation of iPTF16geu in the F110W band obtained on November 17th, 2016. The blue circle marks the bright star visible in all IR observations, that was used for determining the aperture correction.

have been derived. The two sets of values are used both to calculate the aperture correction for the PSF photometry and to assess the quality of this simple time-independent PSF model. The later is quantified by the estimated standard deviation between the PSF and and aperture photometry for all observations in a given filter. These values are then added in quadrature to the photometry error budget.

The fitted parameters and the σ values are given in Table B1 for the different filters. For the WFC3/IR data the last epoch from Nov 22, 2016 was excluded from the fits since this was found to deviate significantly from the others.

APPENDIX C: PHOTOMETRY OF iPTF16geu

Here we present the data tables that the the analysis in this paper is based on.

Table C1. Derived photometry for the four lensed SN images. The first error quoted for each measurement is the statistical uncertainty that is expected to uncorrelated between epochs. This includes the expected PSF variations discussed in §B. The second error, is the systematic error from the background model fit discussed in the text. This is will be correlated for measurements obtained with the same filter.

MJD (days)	Filter	Flux #1 (counts/s)	Flux #2 (counts/s)	Flux #3 (counts/s)	Flux #4 (counts/s)	ZP (mag)
57681.64	$F110W$	4.60E+02 (1E+01,6E+01)	1.84E+02 (8E+00,4E+01)	7.87E+01 (8E+00,4E+01)	6.91E+01 (9E+00,5E+01)	26.64
57681.64	$F160W$	9.11E+01 (6E+00,5E+01)	5.88E+01 (5E+00,4E+01)	2.59E+01 (5E+00,4E+01)	4.47E+01 (6E+00,5E+01)	25.76
57685.91	$F625W$	5.64E+01 (5E+00,2E+00)	1.80E+01 (2E+00,1E+00)	5.62E+00 (8E−01,2E+00)	1.55E+00 (6E−01,2E+00)	25.42
57685.92	$F814W$	1.15E+02 (3E+00,3E+00)	4.05E+01 (1E+00,2E+00)	1.33E+01 (9E−01,2E+00)	6.99E+00 (8E−01,3E+00)	24.99
57685.93	$F475W$	9.16E+00 (1E+00,2E−01)	3.27E+00 (5E−01,2E−01)	1.03E+00 (4E−01,2E−01)	1.70E−02 (3E+00,2E−01)	25.58
57685.94	$F390W$	6.31E−01 (2E−01,3E−02)	1.97E−01 (2E−01,3E−02)	3.56E−01 (2E−01,3E−02)	1.59E−06 (3E−01,3E−02)	25.24
57685.99	$F110W$	3.65E+02 (1E+01,6E+01)	2.14E+02 (9E+00,4E+01)	1.01E+02 (8E+00,4E+01)	5.88E+01 (9E+00,5E+01)	26.64
57685.99	$F160W$	9.45E+01 (9E+00,5E+01)	6.53E+01 (6E+00,3E+01)	3.57E+01 (6E+00,4E+01)	3.71E+01 (7E+00,5E+01)	25.76
57689.91	$F625W$	4.15E+01 (4E+00,2E+00)	1.36E+01 (1E+00,1E+00)	4.24E+00 (6E−01,2E+00)	7.84E−01 (5E−01,2E+00)	25.42
57689.91	$F814W$	9.42E+01 (2E+00,3E+00)	3.35E+01 (1E+00,2E+00)	9.74E+00 (6E−01,2E+00)	5.68E+00 (5E−01,3E+00)	24.99
57689.96	$F110W$	4.69E+02 (1E+01,6E+01)	2.18E+02 (9E+00,4E+01)	8.12E+01 (8E+00,4E+01)	4.04E+01 (9E+00,5E+01)	26.64
57689.96	$F160W$	1.63E+02 (6E+00,5E+01)	7.85E+01 (5E+00,4E+01)	3.08E+01 (5E+00,4E+01)	3.15E+01 (6E+00,5E+01)	25.76
57694.21	$F625W$	3.50E+01 (3E+00,2E+00)	1.17E+01 (1E+00,1E+00)	3.80E+00 (5E−01,2E+00)	4.15E−01 (3E−01,2E+00)	25.42
57694.21	$F814W$	8.73E+01 (2E+00,3E+00)	2.96E+01 (9E−01,2E+00)	9.74E+00 (5E−01,2E+00)	5.39E+00 (4E−01,3E+00)	24.99
57694.24	$F110W$	5.39E+02 (1E+01,6E+01)	1.87E+02 (9E+00,4E+01)	7.31E+01 (8E+00,4E+01)	4.41E+01 (9E+00,5E+01)	26.64
57694.24	$F160W$	2.03E+02 (9E+00,5E+01)	9.53E+01 (6E+00,3E+01)	3.22E+01 (6E+00,4E+01)	4.92E+01 (8E+00,5E+01)	25.76
57698.25	$F625W$	2.98E+01 (3E+00,2E+00)	1.01E+01 (9E−01,1E+00)	3.46E+00 (5E−01,2E+00)	3.96E−01 (4E−01,2E+00)	25.42
57698.25	$F814W$	7.18E+01 (2E+00,3E+00)	2.49E+01 (8E−01,2E+00)	7.60E+00 (5E−01,2E+00)	4.68E+00 (5E−01,3E+00)	24.99
57698.26	$F110W$	4.04E+02 (1E+01,6E+01)	1.56E+02 (8E+00,4E+01)	6.47E+01 (8E+00,4E+01)	4.13E+01 (9E+00,5E+01)	26.64
57698.26	$F160W$	1.75E+02 (7E+00,5E+01)	8.26E+01 (5E+00,4E+01)	3.51E+01 (5E+00,4E+01)	4.84E+01 (6E+00,5E+01)	25.76
57702.16	$F625W$	1.80E+01 (2E+00,2E+00)	8.54E+00 (8E−01,1E+00)	2.86E+00 (4E−01,2E+00)	4.76E−01 (3E−01,2E+00)	25.42
57702.16	$F814W$	6.06E+01 (2E+00,3E+00)	1.95E+01 (7E−01,2E+00)	7.14E+00 (5E−01,2E+00)	3.81E+00 (4E−01,3E+00)	24.99
57702.17	$F110W$	2.75E+02 (1E+01,6E+01)	1.39E+02 (8E+00,4E+01)	5.93E+01 (8E+00,4E+01)	4.61E+01 (9E+00,5E+01)	26.64
57702.17	$F160W$	1.46E+02 (8E+00,5E+01)	7.76E+01 (6E+00,4E+01)	2.66E+01 (6E+00,4E+01)	4.61E+01 (7E+00,5E+01)	25.76
57707.12	$F625W$	1.92E+01 (2E+00,2E+00)	7.13E+00 (7E−01,1E+00)	3.09E+00 (4E−01,2E+00)	9.38E−02 (3E−01,2E+00)	25.42
57707.12	$F814W$	5.00E+01 (1E+00,3E+00)	1.75E+01 (6E−01,2E+00)	6.06E+00 (5E−01,2E+00)	2.98E+00 (4E−01,3E+00)	24.99
57707.14	$F110W$	2.34E+02 (1E+01,6E+01)	1.13E+02 (8E+00,4E+01)	4.99E+01 (7E+00,4E+01)	2.74E+01 (9E+00,5E+01)	26.64
57707.14	$F160W$	1.04E+02 (8E+00,5E+01)	6.67E+01 (5E+00,4E+01)	2.70E+01 (5E+00,4E+01)	4.40E+01 (6E+00,5E+01)	25.76
57709.72	$F625W$	2.21E+01 (2E+00,2E+00)	7.20E+00 (7E−01,1E+00)	2.71E+00 (4E−01,2E+00)	9.75E−02 (3E−01,2E+00)	25.42
57709.74	$F814W$	4.75E+01 (1E+00,3E+00)	1.75E+01 (6E−01,2E+00)	5.66E+00 (4E−01,2E+00)	2.64E+00 (4E−01,3E+00)	24.99
57709.78	$F110W$	1.48E+02 (1E+01,6E+01)	1.12E+02 (8E+00,4E+01)	5.00E+01 (8E+00,4E+01)	2.40E+01 (9E+00,5E+01)	26.64
57709.78	$F160W$	9.06E+01 (7E+00,5E+01)	5.96E+01 (6E+00,4E+01)	2.44E+01 (5E+00,4E+01)	4.14E+01 (7E+00,5E+01)	25.76
57714.32	$F625W$	2.07E+01 (2E+00,2E+00)	6.70E+00 (7E−01,1E+00)	2.81E+00 (4E−01,2E+00)	3.70E−01 (3E−01,2E+00)	25.42
57714.32	$F814W$	4.22E+01 (1E+00,3E+00)	1.48E+01 (6E−01,2E+00)	5.31E+00 (4E−01,2E+00)	2.66E+00 (4E−01,3E+00)	24.99

This paper has been typeset from a TEX/LATEX file prepared by the author.